Analysis of the generalized gradient approximation for the exchange energy

José L. Gázquez [a,*], *Jorge M. del Campo* [b,*], *S. B. Trickey* [c], *Rodrigo J. Alvarez-Mendez* [d], *and Alberto Vela* [d]

[a] Departamento de Química, Universidad Autónoma Metropolitana-Iztapalapa, Av. San Rafael Atlixco 186, México, D. F. 09340 México

[b] Departamento de Física y Química Teórica, Facultad de Química, Universidad Nacional Autónoma de México, México, D. F. 04510 México

[c] Quantum Theory Project, Dept. of Physics and Dept. of Chemistry, P.O. Box 118435, University of Florida, Gainesville FL 32611-8435, USA

[d] Departamento de Química, Cinvestav, Av. IPN 2508, Colonia San Pedro Zacatenco 07360, México, D. F. 07360 México

25 May 2012

* Corresponding authors: jlgm@xanum.uam.mx, jmdelc@unam.mx.

I. Introduction

The framework provided by the Kohn-Sham[1] (KS) form of density functional theory[2] for the electronic structure description of atoms, molecules and solids has become of great importance. Currently available approximations to the exchange-correlation (XC) energy functional allow the study of small, medium and large systems with a reasonable computational effort and quality of outcomes.[3-7] However, the accuracy in the prediction of structural, thermodynamic and kinetic properties, among others, with comparatively simple functionals needs to be increased beyond present limits so as to achieve a reliable method for the description of a wide variety of systems with different characteristics.[8]

A few years ago, Perdew and Schmidt,[9] were able to organize what had been the historical development and some of the issues confronting any attempt at systematic increase of the accuracy of the XC functional, through what they called Jacob's ladder. On it, the local spin density approximation (LDA), in which the functional is determined solely in terms of the local values of the spin up and spin down electronic densities via the expression for the homogeneous electron gas, is placed on the first rung. The second rung consists of functionals that depend, additionally, on the magnitude of the gradients of the spin up and spin down densities, to account for inhomogeneities. Because the form of that dependence is not simply that of the gradient expansion, such functionals are usually referred as generalized gradient approximations (GGA). The third rung comprises functionals that incorporate the Laplacian of the density and/or the KS kinetic energy density. Through the latter, one introduces an explicit dependence on the KS orbitals, additional to the one that comes from expression of the electronic density in terms of these orbitals. On the fourth rung, a fraction or the full exact exchange is incorporated. Recall that the X functional is defined from the KS orbitals, through their implicit dependence on the

density. Global and local hybrid functionals correspond to this level. On the fifth rung, explicit dependence on the unoccupied KS orbitals is added. Second and third rung functionals are said to be of "semi-local" nature (although they are strictly one-point functionals), while fourth and fifth rung functionals have explicitly non-local components.

In the framework of this systematization, the usual expectation, or at least hope, is for the accuracy to increase as one climbs the ladder, although the complexity and computational effort will also increase. However, an interesting aspect is that the actual accuracy limits for a given rung are not necessarily exhausted by the current state of the art at that rung. Lacking an analytical framework by which to assess the ultimately achievable accuracy for some quantity *e.g.* bond lengths or atomization energies, functional developers are forced to exploration of improvement of existing successful approximations.

In this context the search for better descriptions at the GGA rung continues to be a very active research area. In part, this is because such functionals provide good balance between accuracy and computational effort. Interest in GGAs also persists because of the quest for implementation of orbital-free density functional theory.[10,11] Additionally, the GGA functionals usually are ingredients of the higher rung approximations, so that it is important to achieve a better understanding of their general behavior, and the constraints that they could or should satisfy.

The object of the present work is to analyze the behavior of GGA functionals from the perspective of the constraints related with the low and large reduced density gradient regions, taking as starting point the approximation of Perdew, Burke and Ernzerhof (PBE),[12] and to analyze the behavior of the reduced density gradient as a function of the density, to establish some of the implications it may have in the development of improved GGA functionals.

II. The PBE formulation of the generalized gradient approximation for the exchange energy functional

A. PBE and its revisions

The exchange energy functional in the generalized gradient approximation usually is expressed, for the spin non-polarized case, in the form

$$E_x[\rho] = \int d\mathbf{r}\ \rho(\mathbf{r})\ \varepsilon_{xLDA}[\rho(\mathbf{r})]\ F_x(s) \quad , \tag{1}$$

where the X energy density in the LDA is

$$\varepsilon_{xLDA}[\rho(\mathbf{r})] = -C_X \rho^{1/3}(\mathbf{r}) = -(3/4)(3/\pi)^{1/3}\rho^{1/3}(\mathbf{r}) \quad , \tag{2}$$

and the reduced density gradient is defined as

$$s(\mathbf{r}) = \left|\nabla\rho(\mathbf{r})\right| / [2\ (3\pi^2)^{1/3}\ \rho^{4/3}(\mathbf{r})] . \tag{3}$$

The enhancement factor $F_X(s)$ describes deviations from homogeneous electron gas behavior. For PBE, it is written as[12]

$$F_X^{PBE}(s) = 1 + \kappa - \frac{\kappa}{1 + \frac{\mu\ s^2}{\kappa}} \quad , \tag{4}$$

where κ and μ are parameters.

The PBE enhancement factor form, together with the values assigned to the parameters κ and μ, fulfill the following constraints:

(a) Under uniform density scaling, $\rho(\mathbf{r}) \rightarrow \lambda^3\ \rho(\lambda\mathbf{r})$, the exchange energy scales like λ.

(b) From Eq. (4), for $s = 0$, $F_X^{PBE}(0) = 1$, to recover the homogeneous electron gas exchange.

(c) Although written for the spin non-polarized case, the spin-polarized expressions satisfy the spin-scaling relationship

$$E_X[\rho_\uparrow, \rho_\downarrow] = (E_X[2\rho_\uparrow] + E_X[2\rho_\downarrow])/2 \quad , \tag{5}$$

where $\rho_\uparrow$ and $\rho_\downarrow$ are the spin-up and spin-down electron densities.

(d) Being a GGA, the exchange energy and its functional derivative do not diverge for atoms and molecules at the exponential tail of the charge distribution.

(e) The Lieb-Oxford bound[13,14] that establishes the most negative value that the exchange energy may attain for a given electron density, namely,

$$E_X[\rho_\uparrow, \rho_\downarrow] \geq -1.679 \int d\mathbf{r}\ \rho^{4/3}(\mathbf{r}) \tag{6}$$

is satisfied, by imposing the condition that the local values of $F_X(s)$ should not grow beyond a value of 1.804. Since for the form given by Eq. (4), the maximum value of $F_X(s)$ is $1+\kappa$ (the limit when $s \to \infty$), one finds that $\kappa = 0.804$.

(f) From Eq. (4), one has that in the small s regime,

$$F_X(s) \to 1 + \mu\, s^2 \quad , \tag{7}$$

which indicates that μ is directly related to the weight given to the density gradient. Now, the LDA provides a very good description of the linear response of the spin-un-polarized uniform electron gas. Thus, in the PBE functional, μ was set to cancel the second-order gradient contribution to the correlation energy in the high density limit, through the relationship

$$\mu = \pi^2\, \beta / 3 \quad , \tag{8}$$

where, according to Ma and Brueckner,[15] $\beta = 0.066725$, and therefore $\mu_{PBE} = 0.21951$.

The form of the enhancement function given by Eq. (4) was first proposed by Becke,[16] who determined the values of the parameters empirically, through a least squares fit to the Hartree-Fock X energies of the noble gas atoms He-Xe, using Hartree-Fock densities to evaluate the integral in Eq. (1). The values that he found were $\kappa = 0.967$ and $\mu = 0.235$.

The PBE XC functional leads to a reasonable description of a wide variety of properties of molecules and solids. It has become one of the most heavily used approximations in electronic structure calculations. However, several modifications have been proposed, all with the objective of improving the calculated values of various sets of properties.[17-26]

A general finding which emerges from those modifications is that the magnitude of μ is correlated with the prediction of structural, thermodynamic and kinetic properties. The smallest non-empirical value of μ corresponds to the gradient expansion approximation (GEA) value,[27] $\mu_{GEA} = 10/81 \approx 0.12346$, while the largest non-empirical value of μ comes from imposition of the constraint that, for the hydrogen atom, the exchange energy cancels the Coulomb repulsion energy. The later constraint leads[26] to $\mu_{xH} = 0.27583$. Large values of μ are better for atomization energies and worse for crystalline lattice constants, while low values of μ generate the opposite trend. In fact, Zhao and Truhlar[20] also showed that the magnitude of the coefficient μ correlates with the behavior of the cohesive energies of solids, reaction barrier heights, and non-hydrogenic bond distances in small molecules.

It is important to note that, in general, when the value of μ is changed, the value of β is also changed, through Eq. (8), or through other arguments, so that in addition to the exchange energy, the correlation energy also has an impact on this behavior.

B. The large reduced density gradient limit

Most of the PBE modifications have essentially the same behavior at large values of the reduced density gradient, that is, they are built in such a way that $F_x(s) \to 1 + \kappa$ when $s \to \infty$. Their main differences occur in the interval $0 \le s \le 3$, although for larger values of s, the

difference among the different approximations may also come from the different values of κ. Nonetheless, one may wonder about the behavior of the enhancement function in this limit, which arises from the exponential tail of the electronic density of finite systems far away from the nuclei. This was the viewpoint adopted in the development of the VMT[28] X energy functional, which can be viewed as a candidate for superseding PBE. A key analysis in the development of the VMT enhancement factor form involves the outer regions of an atom or a molecule. There the electronic density and its gradient vary slowly and the density is small compared to its peak value. Thus one should recover the homogeneous electron gas type behavior, and therefore VMT was built imposing the condition $F_{xVMT}(s) \to 1$ when $s \to \infty$. However, Levy and Perdew[14] have shown that the exact asymptotic behavior is given by

$$\lim_{s\to\infty} s^{1/2}\ F_{XC}(\rho, s) < \infty \qquad . \tag{9}$$

Since the unpolarized enhancement factor may be expressed in terms of its exchange and correlation components, Eq. (9) separates into

$$\lim_{s\to\infty} s^{1/2}\ F_{X}(s) < \infty \quad , \tag{10}$$

and

$$\lim_{s\to\infty} s^{1/2}\ F_{C}(\rho, s) < \infty \qquad . \tag{11}$$

The limit expressed in Eq. (10) indicates that $F_x(s)$ should decay asymptotically to zero at a rate equal or faster than $s^{-1/2}$. To our knowledge, only the GGA functionals PW91 (Ref. 29), LG (Ref. 30), and the recently proposed VT{8,4} (Ref. 31), based on VMT, satisfy Eq. (10). Although it is generally accepted that the primary range of interest for real systems $0 \le s \le 3$ (Refs. 32-34) and $0 \le r_s \le 10$ (Refs. 32,33), where $r_s = (3/4\pi\rho)^{1/3}$, it has been shown[31] that the imposition of the large s constraint induces subtle, but important changes in the region $0 \le s \le 3$.

One may go back to the original PBE form, Eq. (4), and apply the reasoning that led from VMT to VT{8,4} in order to satisfy the constraint given by Eq. (10). A simple approach that allows one to achieve this goal is to express the enhancement function in the form

$$F_X^{PBE-LS}(s) = F_X^{PBE}(s) - (\kappa + 1)\left(1 - e^{-\alpha s^2}\right) , \qquad (12)$$

since the product in the second term of the right hand side of this equation leads to a term that cancels the $s \to \infty$ limit of $F_X^{PBE}(s)$, and a second term that decays as $(\kappa + 1)e^{-\alpha s^2}$, hence fulfills Eq. (10).

Substitution of Eq. (4) in Eq. (12) gives

$$F_X^{PBE-LS}(s) = 1 + \kappa\left(1 - \frac{1}{1 + \frac{\mu s^2}{\kappa}}\right) - (\kappa + 1)\left(1 - e^{-\alpha s^2}\right) , \qquad (13)$$

and therefore, in the limit $s \to 0$,

$$F_X^{PBE-LS}(s) = 1 + \left(\mu - \alpha(\kappa + 1)\right)s^2 + \ldots . \qquad (14)$$

Thus, incorporation of the correct large-s limit gives an additional parameter α, besides μ and κ. To proceed non-empirically, one may make use of two constraints introduced recently in consideration of modifying the original PBE enhancement factor parameters .

One of the constraints was developed by Constantin *et al.*[24] who made use of the asymptotic expansion of the semiclassical neutral atom,[35-37] which for the exchange energy adopts the form

$$E_X = E_X^{LDA} + d_1 Z + d_2 Z^{2/3} + \ldots , \qquad (15)$$

where Z is the number of electrons (equal to the nuclear charge for a neutral atom), and the coefficients are determined from a numerical analysis that leads to[36,37] $d_1 = -0.2240$ and $d_2 = 0.2467$. Within this approach, one finds that the value of the coefficient for $d_1 = -0.2240$

can be obtained from a modified second-order gradient expansion (MGEA) in which $\mu_{MGEA} = 0.260$. The PBE exchange functional with this value of μ, with $\kappa = 0.804$, and with the PBE correlation functional with a value of $\beta = 3\,\mu_{MGEA}/\pi^2 = 0.07903$ was named APBE. It provides an improvement in the description of atomization energies compared to original PBE.

The other constraint,[26] addresses the issue of inadequate cancellation of spurious self-interaction. The constraint is that for one-electron systems with $\rho_1(\mathbf{r})$, the one-electron density, the exact exchange energy must cancel the Coulomb repulsion energy,

$$E_X[\rho_1] = -J[\rho_1] \quad . \tag{16}$$

One can use this equation with the hydrogen atom electron density to fix the value of μ, for $\kappa = 0.804$, with the enhancement function of original PBE form, Eq. (4). The value obtained from that procedure is $\mu_{xH} = 0.27583$. Use of those μ and κ parameters in the PBE X form, together with the PBE correlation with $\beta = 3\,\mu_{xH}/\pi^2 = 0.08384$ leads to a functional that was called PBEmol, because at the GGA rung, it provides a good description of several molecular properties, specially the atomization energies. In essence, PBEmol is the molecular counterpart to PBEsol, in the sense summarized above. Increasing μ favors finite system accuracy at the cost of worsening extended system accuracy and conversely.

We return to the task of setting the three parameters, μ, κ and α, in Eq. (13). We assume first, that the correct value of the coefficient of the second order gradient expansion in the limit $s \to 0$ is the one that arises from the asymptotic expansion of the semiclassical neutral atom. Therefore, from Eq. (14) one has $\mu_{MGEA} = \mu - \alpha\left(\kappa + 1\right) = 0.26$. The second constraint we enforce is freedom from one-electron self-interaction error, Eq. (16), for the hydrogen atom density $\rho_H(r) = \pi^{-1} e^{-2r}$. The third constraint is to enforce the local Lieb-Oxford bound at the maximum

$s_{\max}$ of the function given by Eq. (13), that is $F_X^{PBE-LS}(s_{\max}) = 1.804$. These three requirements yield $\mu = 0.26151$, $\kappa = 0.9403$ and $\alpha = 0.00078$. Within this procedure the value of the coefficient associated with the second order gradient correction to the correlation energy β, could be fixed through Eq. (8) and Eq. (14), so that $\beta_{PBE-LS} = 3\,\mu_{MGEA}/\pi^2 = 0.07903$.

A comparison between several forms of the X enhancement function is given in Figs. (1) and (2). In both, we present a plot for a large interval of values of s, and a plot for the interval $0 \le s \le 3$, in order to distinguish differences in this region.

Fig. (1) compares PBE, PBE-LS, VMT and VT{8,4}. One sees that in the interval $0 \le s \le 3$, PBE-LS is larger than all of the others, and that VMT and VT{8,4},which are similar to each other, also lie above PBE. However, as s grows, PBE-LS goes to zero more rapidly than VT{8,4}, VMT tends to unity (by design), and PBE tends to 1.804. Fig. (2) provides comparison among PBE, PBE-LS, B88[38], and OPTX.[39] The enhancement function for the latter functional, proposed by Handy and Cohen, is

$$F_X^{OPTX}(s) = a_1 + a_2\, c_2 \left[\frac{\gamma\, c_1\, s^2}{1 + \gamma\, c_1\, s^2} \right]^2 , \qquad (17)$$

where $c_1 = 4(6\pi^2)^{2/3}$, $c_2 = (2^{1/3} C_X)^{-1}$, and the parameters a_1, a_2 and γ are fixed through a fitting of the Hartree-Fock energy for the atoms H-Ar. The results are $a_1 = 1.05151$, $a_2 = 1.43169$ and $\gamma = 0.006$. Although this functional has a semiempirical nature, when combined with the correlation energy functional of Lee, Yang and Parr[40] (LYP), it leads to a very good description of several molecular properties, so it is interesting to compare it with the PBE type approximations to analyze the differences among them. Thus, one can see (Fig. 2) that, at $s = 0$, the OPTX enhancement function differs from unity, and that, for values of s between zero and approximately 0.5, OPTX remains practically constant. Thus, in this approximation and

in this interval, the contributions due to the non-uniformities of the density are essentially constant and larger than those provided by X functionals with quadratic behavior. For values of s beyond 0.5, OPTX grows abruptly towards its $s \to \infty$ limiting value $F_X^{OPTX}(s) \to a_1 + a_2 c_2 = 2.59$. On the other hand, one can see that PBE and PBE-LS, in comparison with OPTX, grow slower, starting from unity, in the interval $0 \le s \le 3$. In contrast, the widely used B88 X enhancement function[38] was formulated to yield the correct asymptotic limit of the exchange energy density per electron, namely, $\lim_{r\to\infty} \varepsilon_x = -1/2r$. However, it has been shown[41] that for a GGA this condition is equivalent to $\lim_{s\to\infty} F_{xGGA}(s) \to s/\ln s$, which clearly is irreconcilable with Eq. (10). In Fig. (2) one can see that B88 lies between PBE and PBE-LS in the interval from $s = 0$ to $s \approx 2.5$, and after that it grows abruptly. Separately, it has been shown[42] that this asymptotic growth constraint $\lim_{s\to\infty} F_{xGGA}(s) \to s/\ln s$ is, in fact, irrelevant to the energetic behavior of a GGA, which is why both VT{8.4} X and the PBE-LS proposed here ignore that constraint and use the relevant one, Eq. (10).

C. Results for several atomic and molecular properties

To analyze the performance of the functionals described in the previous section, we consider several atomic and molecular properties. The calculations were done with a developmental version of NWChem vers. 6.0 (Ref. 43).

Table I shows the exchange energies for the atoms H-Ar obtained from exchange only calculations with a Def2-QZVP basis set for several functionals, in comparison with the Hartree-Fock values obtained for the same basis set. One can see, as expected, that the empirical functionals OPTX and B88, whose parameters were set through least squares fits to the exchange energy of atoms He-Ar, lead to the lowest Mean Absolute Errors (MAE). In fact, OPTX with

three adjustable parameters leads to the best description, followed by B88 that has only one adjustable parameter. On the other hand, one can also see that the three non-empirical functionals VMT, VT{8,4}, and PBE-LS, whose enhancement function tends to one, zero, and zero, respectively, in the $s \to \infty$ limit, provide an improvement over the original PBE functional, which is rather similar for the three functionals. We have also included the non-empirical functional revTPSS,[44] which is a meta-GGA, and therefore belongs to the next rung in the Perdew-Schmidt Jacob's ladder. One can see that the results provided by revTPSS are close to the ones obtained from the three large-s corrected GGA functionals.

In Table II we present the results for heats of formation, ionization potentials, electron affinities, proton affinities, binding energies of weakly interacting systems, barrier heights for hydrogen and non-hydrogen transfer reactions, bond distances and harmonic frequencies, for some well known test sets designed to validate energy functionals. Those have been described in previous work.[26,31] In these cases, correlation energy functionals have been added to the exchange energy functionals discussed. Thus, OPTX and B88 X have been combined, as is usual, with LYP C, while PBE, VMT, VT{8,4}, and PBE-LS have been combined with PBE C, to maintain their non-empirical nature. As previously described, for PBE-LS $\beta_{PBE-LS} = 3\,\mu_{MGEA} / \pi^2 = 0.07903$. One can see that except for the electron affinities, the proton affinities and the binding energies of weakly interacting systems, OLYP provides the best description. Particularly, the MAE for the heats of formation is just about one kcal/mol above the value for revTPSS, and the barrier heights have the lowest MAE, including even revTPSS. In the case of the non-empirical functionals, it may be observed that, heats of formation and barrier heights show smaller MAEs for VMT, VT{8,4} and PBE-LS, than PBE, with the best results

corresponding to PBE-LS. However, PBE provides smaller MAEs for bond distances and frequencies.

III. Behavior of the reduced density gradient as a function of the density

The foregoing analysis indicates that it is important to get a closer picture of the behavior of the density and its gradient in different regions of a molecule. To do this, one can follow the procedure of Johnson *et al.,*[45,46] in which the reduced gradient given by Eq. (3) is plotted against the electronic density. Although their objective was to reveal the non-covalent interactions, the plot provides significant information about all regions of a molecule. Thus, in Fig. 3 we present these type of plots for the water molecule, its dimer, and its tetramer, and in Fig. 4 we present the plots corresponding to the reactant, transition state and product of the isomerization reaction of HCN. The calculations reported in this section were carried out with a developmental version of deMon2k, vers. 3.x (Ref. 47)

For the analysis of these plots is important to consider the behavior of the electronic density near the nuclei and far from them. That is,[48,49] for a spherically averaged density we have that at a given nucleus *a* of nuclear charge Z_a,

$$\left.\frac{\partial\ \rho(r)}{\partial r}\right|_{r=0} = -2\ Z_a\ \rho(0) \quad , \tag{18}$$

and, asymptotically, at large distances from the nuclei,[50,51]

$$\rho(r) \xrightarrow[r\to\infty]{} e^{-2(2I)^{1/2} r} \quad , \tag{19}$$

where I is the first ionization potential.

The overall shape of the graph follows a $\rho^{-1/3}$ pattern due to the piecewise exponential nature of the electronic density. With respect to the values of ρ one can identify three approximate regions:

Region I, where ρ takes values between zero and approximately 0.1

Region II, where ρ takes values between approximately 0.1 and 0.8

Region III, where ρ takes values beyond approximately 0.8

Thus, the regions near the nuclei will appear towards the right edge of the graph, in region III, and will be governed by an exponential fall that satisfies Eq. (18) at each nucleus, while the regions far from the nuclei will appear in the upper part of the left edge, in region I, and will be governed by the exponential form given in Eq. (19). Note that in this limit the reduced density gradient diverges, because the density raised to the 4/3 power (denominator) decays faster to zero than the gradient of the density (numerator).

The spikes that appear are a very important aspect in the regions that correspond to small s values, because these correspond to the different chemical interactions present. For all cases, the spikes show that in these regions, the density gradient approaches zero, and becomes equal to zero at the critical point. In Fig. 3, the spikes located in region II reveal the covalent interactions that correspond to regions with intermediate values of the density and low values of the gradient of the density, while the spikes located in region I reveal the noncovalent interactions. They correspond to regions with low values of both the density and its gradient. In Figs. 4 one can see that the covalent bond between carbon and nitrogen basically remains constant at a value of the density slightly over 0.4, while the H-C bond in the reactant and the N-H bond in the product, appears slightly below, and slightly above a value of the density of 0.3, respectively. However, at the transition state, this spike moves to a value slightly below 0.2, that is, it moves towards the

noncovalent interactions region, because at this stage of the interaction the H-C bond is breaking and the N-H bonds is forming, so that in general one could infer that there is a weak interaction of the entity formed by carbon and nitrogen with hydrogen.

Let us consider now the density of the reduced density gradient, $g(s)$. It provides, for a given electronic density, the number of electrons with the values of s that lie between s and $s + ds$. Zupan *et al.*[32,33] have defined this distribution as

$$g(s) = \int d\mathbf{r}\ \rho(\mathbf{r})\ \delta(s - s(\mathbf{r})) \quad , \tag{20}$$

where $\delta(s - s(\mathbf{r}))$ is the Dirac delta function. In Figs. (5) and (6) we present plots of $g(s)$ for the water systems considered here and the isomerization reaction of HCN, respectively (details of the numerical procedure are given in Ref. 34). It is clear from these plots, and from the plots for many others we have done, that the region of physical interest for real systems lies primarily in the interval $0 \le s \le 3$.

IV. Concluding remarks

The study of the GGA functionals considered in this work, and the analysis of the behavior of the reduced density gradient as a function of the electronic density, together with its density, allows one to observe two important aspects for the possible improvement of exchange energy functionals that only depend on the density and its gradient.

The first one is that the contribution to the exchange energy seems to be dominated by the behavior of the enhancement function in the interval $0 \le s \le 3$, and that its description in this region is crucial to improve the accuracy of the non-empirical GGA approximations known to date. However, this behavior does not imply that the imposition of constraints related with large

values of s, like the one given by Eq. (10), are not important. Indeed, we have found in a previous work[31] and in the present one, that by imposing the large-s constraint, one induces changes in the interval $0 \le s \le 3$, which may have an important impact on the prediction of diverse properties. In fact, the results presented in this work, together with the ones reported in Ref. 26, indicate that PBE-LS provides the best description for most of the properties considered. Note also that in its development the constraints associated with Eqs. (15) and (16) were also incorporated, adding to the ones already present in PBE.

The second important aspect of the present analysis comes from the plots of the reduced density gradient versus the density. It was shown that there are two regions of the electronic density that give rise to low values of s. One of those corresponds to the covalent interactions, and one corresponds to the non-covalent or to the transition-state type interactions. This situation could indicate that the weight given to the gradients of the density could be different, depending on the values of the density itself, and that the limit for small s could be revised and modified. Recall that the functional OPTX, that leads to a rather good description of the heats of formation, behaves as s^4 for small s, in contrast with PBE that behaves as s^2.

In summary, the analysis presented here points at some of the issues that may be studied to improve the accuracy of the GGA approximations known to date.

Acknowledgements

We dedicate this work to Prof. B.M. Deb on his seventieth birthday, for his great contributions to the development of theoretical chemistry. We thank the Laboratorio de Supercómputo y Visualización of Universidad Autónoma Metropolitana-Iztapalapa and DGTIC-UNAM for the

use of their facilities. JMC and RJAM were supported in part by Conacyt through a postdoctoral and a doctoral fellowship, respectively. AV, JLG and JMC were supported in part by the Conacyt project grant 128369. JMC was also supported in part by DGAPA-UNAM under Grant No. IA101512. SBT was supported in part by the U.S. Dept. of Energy grant DE-SC-0002139. Part of this work was done while AV was on a sabbatical leave at UAM-Iztapalapa, occupying the "Raul Cetina Rosado" chair, and while JMC was an invited professor in this same institution. They thank all members of the Fisicoquímica Teórica group for their warm hospitality and the intense discussions during their stay.

References

(1) Kohn, W.; Sham, L. J. *Phys. Rev.* **1965**, *140*, A1133.

(2) Hohenberg, P.; Kohn, W. *Phys. Rev. B* **1964**, *136*, B864.

(3) Parr, R. G.; Yang, W. T. *Density-Functional Theory of Atoms and Molecules*; Oxford University Press: New York, 1989.

(4) Dreizler, R. M.; Gross, E. K. U. *Density Functional Theory*; Springer: Berlin, 1990.

(5) Perdew, J. P.; Kurth, S. in *A Primer in Density Functional Theory*; Fiolhais, C., Nogueira, F., Marques, M. A. L., Eds.; Springer: Berlin, 2003; pp 1.

(6) Perdew, J. P.; Ruzsinszky, A.; Tao, J. M.; Staroverov, V. N.; Scuseria, G. E.; Csonka, G. I. *J. Chem. Phys.* **2005**, *123*, 062201.

(7) Scuseria, G. E.; Staroverov, V. N. in *Theory and Applications of Computational Chemistry: The First Forty Years*; Dykstra, C., Frenking, G., Kim, K. S., Scuseria, G. E., Eds.; Elsevier:

Amsterdam, 2005; pp 669.

(8) Cohen, A. J.; Mori-Sanchez, P.; Yang, W. T. *Chem. Rev.* **2012**, *112*, 289.

(9) Perdew, J. P.; Schmidt, K. in *Density Functional Theory and its Application to Materials*; Van Doren, V. E., Van Alsenoy, C., Geerlings, P., Eds.; AIP, Melville: New York, 2001; pp 1.

(10) Dufty, J. W.; Trickey, S. B. *Phys. Rev. B* **2011**, *84*, 125118.

(11) Trickey, S. B.; Karasiev, V. V.; Vela, A. *Phys. Rev. B* **2011**, *84*, 075146.

(12) Perdew, J. P.; Burke, K.; Ernzerhof, M. *Phys. Rev. Lett.* **1996**, *77*, 3865; erratum **1997**, *78*, 1396.

(13) Lieb, E. H.; Oxford, S. *Int. J. Quantum Chem.* **1981**, *19*, 427.

(14) Levy, M.; Perdew, J. P. *Phys. Rev. B* **1993**, *48*, 11638; erratum **1997**, *55*, 13321.

(15) Ma, S. K.; Brueckner, K. A. *Phys. Rev.* **1968**, *165*, 18.

(16) Becke, A. D. *J. Chem. Phys.* **1986**, *84*, 4524.

(17) Zhang, Y. K.; Yang, W. T. *Phys. Rev. Lett.* **1998**, *80*, 890.

(18) Hammer, B.; Hansen, L. B.; Norskov, J. K. *Phys. Rev. B* **1999**, *59*, 7413.

(19) Perdew, J. P.; Ruzsinszky, A.; Csonka, G. I.; Vydrov, O. A.; Scuseria, G. E.; Constantin, L. A.; Zhou, X. L.; Burke, K. *Phys. Rev. Lett.* **2008**, *100*, 136406.

(20) Zhao, Y.; Truhlar, D. G. *J. Chem. Phys.* **2008**, *128*, 184109.

(21) Swart, M.; Sola, M.; Bickelhaupt, F. M. *J. Chem. Phys.* **2009**, *131*, 094103.

(22) Cooper, V. R. *Phys. Rev. B* **2010**, *81*, 161104.

(23) Fabiano, E.; Constantin, L. A.; Della Sala, F. *Phys. Rev. B* **2010**, *82*, 113104.

(24) Constantin, L. A.; Fabiano, E.; Laricchia, S.; Della Sala, F. *Phys. Rev. Lett.* **2011**, *106*, 186406.

(25) Fabiano, E.; Constantin, L. A.; Della Sala, F. *J. Chem. Theory Comput.* **2011**, *7*, 3548.

(26) M. del Campo, J.; Gázquez, J. L.; Trickey, S. B.; Vela, A. *J. Chem. Phys.* **2012**, *136*, 104108.

(27) Antoniewicz, P. R.; Kleinman, L. *Phys. Rev. B* **1985**, *31*, 6779.

(28) Vela, A.; Medel, V.; Trickey, S. B. *J. Chem. Phys.* **2009**, *130*, 244103.

(29) Perdew, J. P. in *Electronic Structure of Solids '91*; Ziesche, P., Eschrig, H., Eds.; Akademie: Berlin, 1991; pp 11.

(30) Lacks, D. J.; Gordon, R. G. *Phys. Rev. A* **1993**, *47*, 4681.

(31) Vela, A.; Pacheco-Kato, J. C.; Gázquez, J. L.; M. del Campo, J.; Trickey, S. B. *J. Chem. Phys.* **2012**, *136*, 144115.

(32) Zupan, A.; Perdew, J. P.; Burke, K. *Int. J. Quantum Chem.* **1997**, *61*, 835.

(33) Zupan, A.; Burke, K.; Emzerhof, M.; Perdew, J. P. *J. Chem. Phys.* **1997**, *106*, 10184.

(34) M. del Campo, J.; Gázquez, J. L.; Alvarez-Mendez, R. J.; Vela, A. *Int. J. Quantum Chem.*, in press.

(35) Perdew, J. P.; Constantin, L. A.; Sagvolden, E.; Burke, K. *Phys. Rev. Lett.* **2006**, *97*, 223002.

(36) Elliott, P.; Burke, K. *Can. J. Chem.-Rev. Can. Chim.* **2009**, *87*, 1485.

(37) Lee, D.; Constantin, L. A.; Perdew, J. P.; Burke, K. *J. Chem. Phys.* **2009**, *130*, 034107.

(38) Becke, A. D. *Phys. Rev. A* **1988**, *38*, 3098.

(39) Handy, N. C.; Cohen, A. J. *Mol. Phys.* **2001**, *99*, 403.

(40) Lee, C. T.; Yang, W. T.; Parr, R. G. *Phys. Rev. B* **1988**, *37*, 785.

(41) van Leeuwen, R.; Baerends, E. J. *Phys. Rev. A* **1994**, *49*, 2421.

(42) Engel, E.; Chevary, J. A.; Macdonald, L. D.; Vosko, S. H. *Z. Phys. D: At. Mol. Clusters* **1992**, *23*, 7.

(43) Valiev, M.; Bylaska, E. J.; Govind, N.; Kowalski, K.; Straatsma, T. P.; Van Dam, H. J. J.; Wang, D.; Nieplocha, J.; Apra, E.; Windus, T. L.; de Jong, W. *Comput Phys Commun* **2010**, *181*, 1477.

(44) Perdew, J. P.; Ruzsinszky, A.; Csonka, G. I.; Constantin, L. A.; Sun, J. W. *Phys. Rev. Lett.* **2009**, *103*, 026403; erratum **2011**, *106*, 179902.

(45) Johnson, E. R.; Keinan, S.; Mori-Sanchez, P.; Contreras-Garcia, J.; Cohen, A. J.; Yang, W. T. *J. Am. Chem. Soc.* **2010**, *132*, 6498.

(46) Contreras-Garcia, J.; Johnson, E. R.; Keinan, S.; Chaudret, R.; Piquemal, J. P.; Beratan, D. N.; Yang, W. T. *J. Chem. Theory Comput.* **2011**, *7*, 625.

(47) Koster, A. M.; Geudtner, G.; Calaminici, P.; Casida, M. E.; Domínguez, V. D.; Flores-Moreno, R.; Gamboa, G. U.; Goursot, A.; Heine, T.; Ipatov, A.; Janetzko, F.; M. del Campo, J.; Reveles, J. U.; Vela, A.; Zuniga-Gutierrez, B.; Salahub, D. R. *deMon2k*, *version 3.x*, *The deMon developers*, Cinvestav, Mexico City, 2011.

(48) Kato, T. *Commun. Pure Appl. Math.* **1957**, *10*, 151.

(49) Steiner, E. *J. Chem. Phys.* **1963**, *39*, 2365.

(50) Morrell, M. M.; Parr, R. G.; Levy, M. *J. Chem. Phys.* **1975**, *62*, 549.

(51) Katriel, J.; Davidson, E. R. *Proc. Natl. Acad. Sci. USA* **1980**, *77*, 4403.

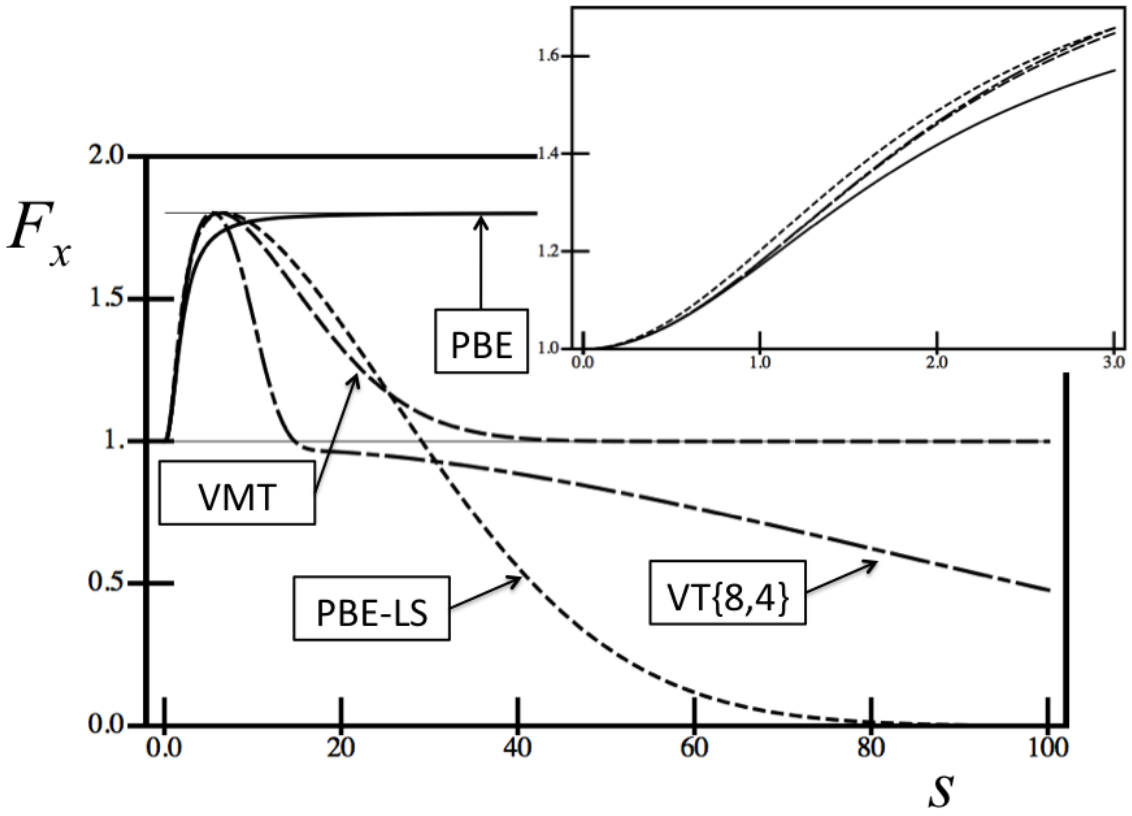

Fig. 1. Plot of the enhancement factor as a function of the reduced density gradient for PBE, VMT, VT{8,4}, and PBE-LS. The inset corresponds to a zoom in the range of interest for real systems.

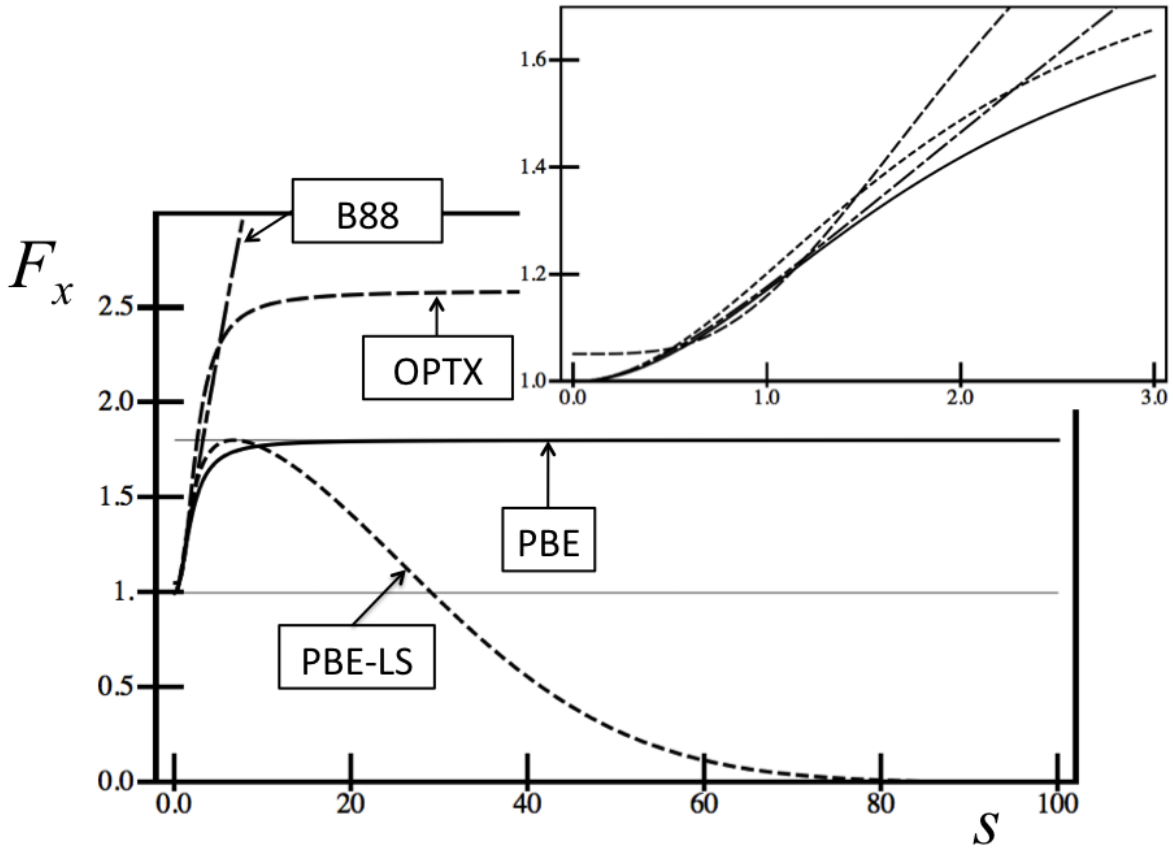

Fig. 2. Plot of the enhancement factor as a function of the reduced density gradient for PBE, OPTX, and PBE-LS. The inset corresponds to a zoom in the range of interest for real systems.

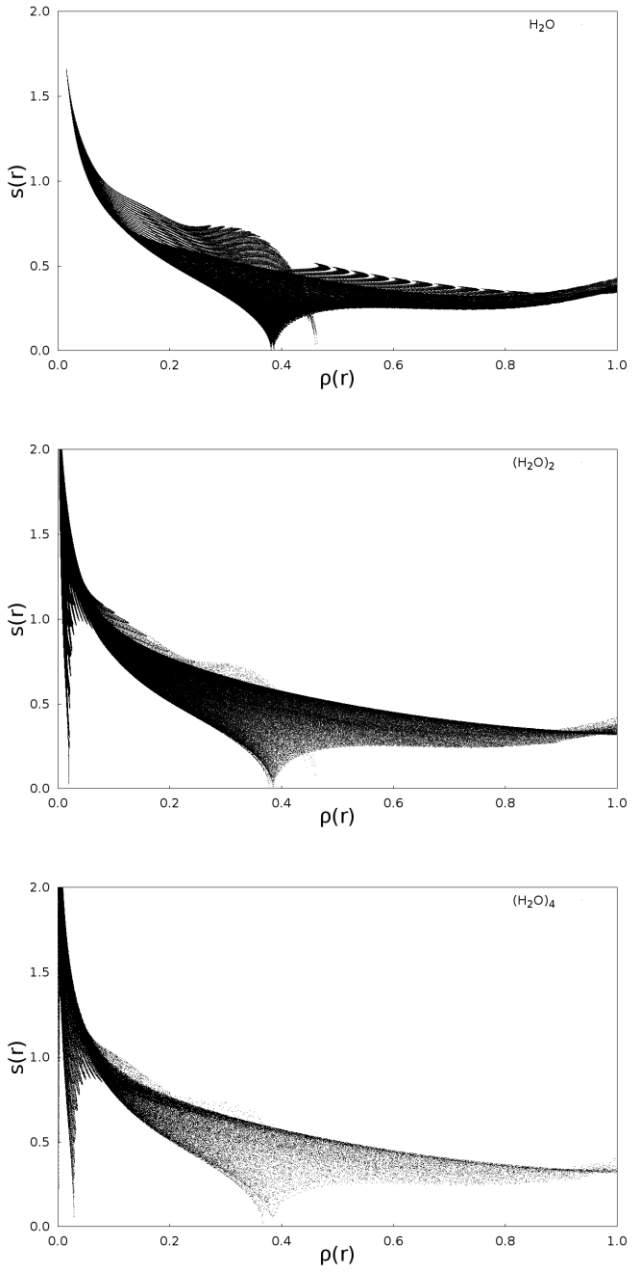

Fig. 3. Plot of the reduced density gradient versus the electronic density for water molecule (top), its dimer (middle) and its tetramer (bottom).

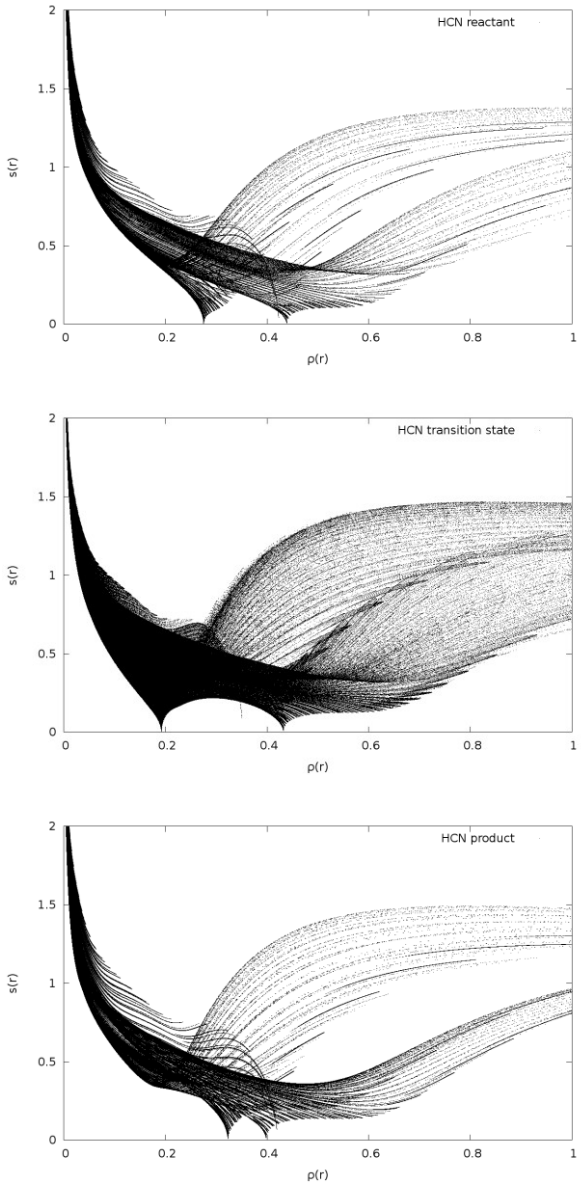

Fig. 4. Plot of the reduced density gradient versus the electronic density for the reactant (top), transition state (middle) and product (bottom) of the isomerization reaction of the HCN molecule.

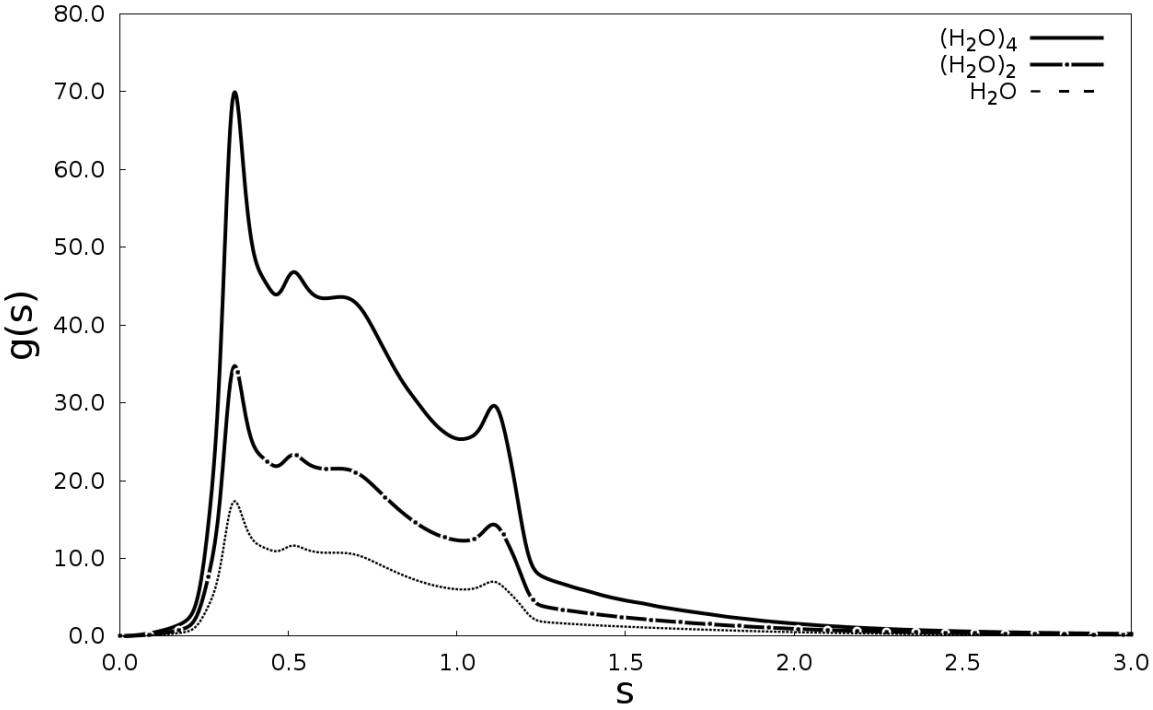

Fig. 5. Plot of the density of the reduced density gradient as a function of *s* for the water systems considered in this work.

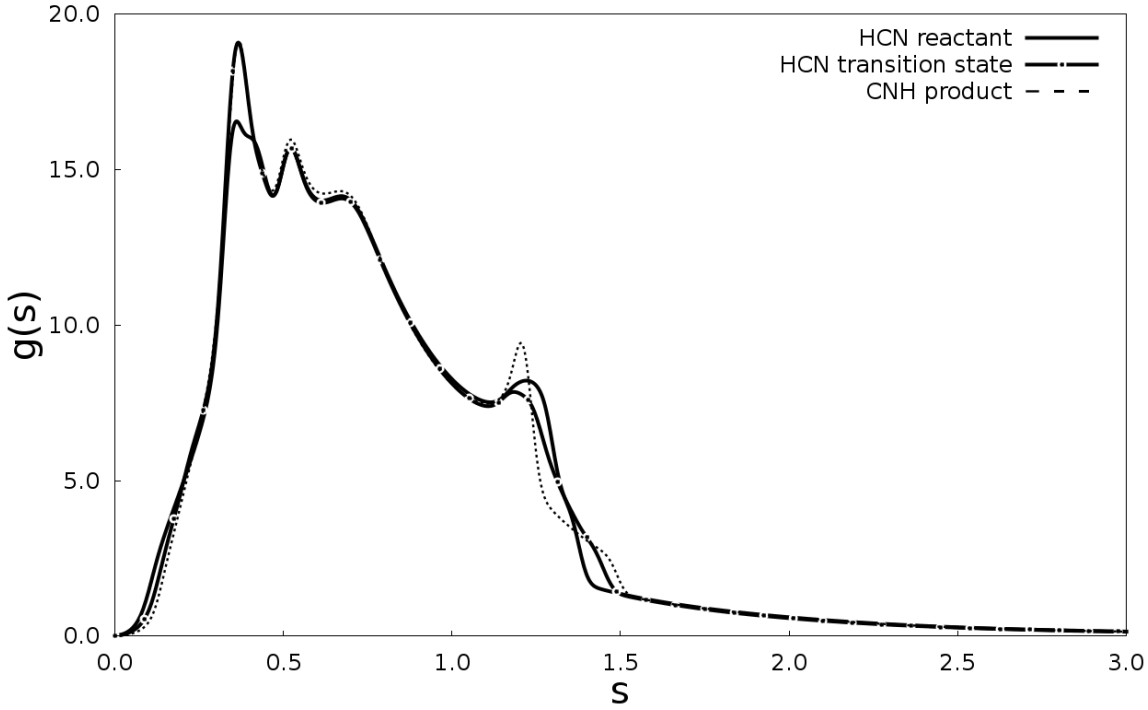

Fig. 6. Plot of the density of the reduced density gradient as a function of *s* for the isomerization reaction of HCN.

TABLE I. Exchange energies and mean absolute errors (MAE) with respect to the Hartree-Fock values, in hartree units, as determined with several GGA functionals and one meta-GGA through exchange-only calculations.

	Exchange energy							
Atom	HF	OPTX	B88	PBE	VMT	VT{8,4}	PBE-LS	revTPSS
H	-0.313	-0.308	-0.306	-0.301	-0.304	-0.304	-0.310	-0.311
He	-1.026	-1.019	-1.016	-1.002	-1.010	-1.011	-1.029	-1.025
Li	-1.781	-1.775	-1.768	-1.748	-1.761	-1.762	-1.791	-1.783
Be	-2.667	-2.663	-2.652	-2.627	-2.645	-2.647	-2.690	-2.671
B	-3.770	-3.754	-3.748	-3.716	-3.738	-3.740	-3.799	-3.775
C	-5.077	-5.054	-5.048	-5.008	-5.034	-5.036	-5.111	-5.065
N	-6.607	-6.584	-6.569	-6.521	-6.549	-6.551	-6.643	-6.578
O	-8.218	-8.190	-8.188	-8.131	-8.162	-8.165	-8.279	-8.198
F	-10.045	-10.016	-10.021	-9.954	-9.988	-9.990	-10.125	-10.012
Ne	-12.108	-12.088	-12.087	-12.009	-12.044	-12.047	-12.201	-12.060
Na	-14.017	-13.989	-13.977	-13.891	-13.930	-13.933	-14.108	-13.944
Mg	-15.994	-15.968	-15.954	-15.863	-15.905	-15.908	-16.105	-15.907
Al	-18.092	-18.068	-18.055	-17.952	-17.997	-18.000	-18.220	-17.992
Si	-20.304	-20.281	-20.261	-20.147	-20.194	-20.198	-20.440	-20.180
P	-22.642	-22.627	-22.593	-22.467	-22.517	-22.521	-22.784	-22.493
S	-25.034	-25.014	-24.976	-24.837	-24.889	-24.893	-25.180	-24.865
Cl	-27.544	-27.529	-27.481	-27.329	-27.384	-27.388	-27.698	-27.349
Ar	-30.185	-30.185	-30.119	-29.953	-30.011	-30.015	-30.347	-29.964
MAE		0.017	0.034	0.109	0.076	0.073	0.080	0.071

TABLE II. Mean absolute errors (MAE) for several properties as calculated with several GGA functionals and one meta-GGA. All energies are in kcal/mol, bond distances in Å, and frequencies in cm^{-1}. The number of cases for each test set appears in parenthesis.

	MAE						
Property	OLYP	BLYP	PBE	VMT	VT{8,4}	PBE-LS	revTPSS
Heats of formation (223)	5.51	9.64	21.21	10.53	9.98	9.39	4.55
Ionization potentials (13)	2.61	4.20	3.47	3.26	3.25	3.65	3.06
Electron affinities (13)	3.63	2.97	2.64	2.48	2.48	2.61	2.45
Proton affinities (8)	1.66	1.78	1.39	1.07	1.09	1.23	1.80
Binding energies of weakly interacting systems (31)	2.27	1.67	1.64	1.52	1.53	1.49	1.41
Reaction barrier heights:							
Hydrogen transfer forward (19)	6.02	7.81	9.49	8.31	8.23	7.26	6.63
Hydrogen transfer backward (19)	6.06	7.85	9.72	8.66	8.59	7.77	7.72
Non-hydrogen transfer forward (19)	7.74	10.49	10.38	9.82	9.79	9.45	11.18
Non-hydrogen transfer backward (19)	7.21	10.03	9.96	9.49	9.46	9.31	10.08
Bond distances (96)	0.0198	0.0240	0.0179	0.0209	0.0211	0.0216	0.0204
Frequencies (82)	40.42	56.25	43.30	45.41	45.57	45.74	39.58